Noname manuscript No.
(will be inserted by the editor)

Resizing Geovisualization with Density Map via a Map Collage

Junjie Chen · Changbo Wang · Chenhui Li

Received: date / Accepted: date

Abstract The extensive distribution of portable digital devices brings demands of adapting media to restricted display spaces or various aspect ratios. Most existing content-aware visualization resizing approaches introduce nonlinear deformation to enhance or preserve salient areas while squeezing non-salient ones. Their deformation on image-based geographic context could cause confusion and make it harder to interpret by the general user. In this paper, we describe a deformation-free approach to resize the geovisualization using density map, resulting in a collage layout of maps, called map collage. We show our technique of constructing a collage layout for one frame of geospatial data and a strategy of extending it to the temporal dimension. We demonstrate the results on two sets of geotemporal data and conducted a survey comparing our method, the seam carving, and the uniform scaling, which shows that ours is better than the other two.

Keywords visualization resizing · geovisualization · spatial-temporal data · density map · information visualization

1 Introduction

In supporting collaborative visual analysis across multiple platforms, visualizations require suitable resizing approaches to be adapted to various displays, mostly small-sized screens of portable devices. Many works have been introduced to various types of visualizations. Some resizing approaches treat a visualization as image and perform deformation when scaling their display size [18, 33], some tweak the layout of a visualization based on the source data. Map is a key component in geovisualizations where geospatial data are mapped. However, many existing resizing approaches introduce nonlinear deformation to the map, which brings extra cognitive loads or probable misinterpretation, especially to users who are used to the maps based on the widely used Mercator projection [1]. Thus, we aim to propose a geovisualization resizing method targeting the general audience, which dose not introduce nonlinear deformation further than the original projection.

One simple approach to resize a map on small mobile screens is the uniform scaling. By pinching on a touchscreen, user could zoom in onto interesting locations. To compare the data of multiple different locations, user could, if such functions are provided, add them into a list and switch among them, or zoom out to an overview degree. The former interaction preserves almost no mental map other than transition animations panning the map between locations. It falls to the users to memorize the data of the former location. As for the second way, zooming out makes graphic type of visual encoding, such as density map, smaller and thus harder to recognize.

In this paper, we present a technique, called map collage, to resize the geovisualizations to smaller display spaces or different aspect ratios while bringing no further deformation other than original Mercator projection. Specifically, we focus on the density maps generated by kernel density estimation (KDE) [17], which represents an estimation of the spatial distribution of data in the manner of a colorized overlay. The important regions with their geographical contexts, i.e. underlaying maps, are cropped and stitched together to form a collage-style layout with constrained relative positions. Our proposed technique aims to compensate the readability of the geovisualizations on small screens as a simplification tool. We then extend the map collage to the temporal dimension, enabling users to switch among frames. The main challenge arises from the difference of geospatial data between adjacent frames. To alleviate the impact of sudden jumps of important

Junjie Chen · Changbo Wang · Chenhui Li
East China Normal University, Shanghai, China.

regions, we first generate an initial global collage layout containing all important regions of all frames and then adjusted for each frame to fit. Simple transition animation between two frames helps users to follow the jumps.

The contributions of our work are summarized as follows:

1. Presenting a new deformation-free resizing approach of geovisualization that uses density map, generating a collage layout of maps that shows important region in each cell of the target display space.
2. Designing a heuristic method extending the collage layout to the temporal dimension for geotemporal data browsing.
3. Raising the problem of deformation-free resizing visualization of geotemporal data for the first time and proposing an approach for it.

2 Related Work

Image Resizing. A geovisualization with its density map could be regarded as a static image, so that image resizing approaches could be applied onto it. Among content-aware image resizing methods, seam carving [3] was the first pixel-based method. It computes monotonic seams of pixels to be inserted or removed, achieving a variety of image manipulations. Subsequently, Rubinstein et al. [26] extended this work to video retargeting. Mesh-based resizing approaches such as those presented by Wang et al. [31], and Wolf et al. [32] deform images by nonlinear grid warping. These perception-based image resizing depends on image recognition where the result of visual saliency is conveyed via a saliency map that identifies the importance of each pixel. Guided by the saliency map, these image resizing methods provides continuous control of the underlying image. The regions in images with low-salient pixels are tend to be shrunk or removed, and shapes and sizes of the regions with high-salient pixels are tend to be preserved.

Visualization Resizing. The perception-based techniques could be transplanted to various types of visualization with specifically designed saliency metrics. Some types of visualization may share the same traits, allowing generic resizing solutions. ViSizer [33] combines a degree of interest (DOI) map [10] and a clutter map for computing a significance map of the visualization. Li et al. [18] proposed an multilayer saliency model called visual saliency map (VSM) describing the important regions and the context of a visualization, and then constructs an adaptive triangulation grid to deform information visualizations, including those with geographic context.

Cartograms. Cartograms combine geographic context with geo-referenced statistic information by scaling geographic regions proportional to statistical values. A survey [23] categorizes cartograms broadly into four types: contiguous, non-contiguous, Doring and rectangular. Contiguous cartograms usually nonlinearly deform shapes of geographic regions [9, 11, 15]. The Doring [6] and the rectangular [5] ones preserve no geographic shapes at all.

Cartograms save space by integrating and summary by administration regions, so the detailed data distribution within regions is not preserved. Even if the distribution is preserved, the hotspots are separated by administration borders. Our method, on the other hand, display the original distribution of the hotspots and separate them by density.

Similar to cartograms but different, PixelMaps [16] deforms map according to the distribution of spatial points but not statistics values. However, it's hard for the general audience to relate the dramatically deformed result to the original map.

Focus + Context. Techniques of focus + context also involve content enhancement and deformation, which are related to resizing and adapting. They could retain sizes of important regions of a downward-resized visualization. Fisheye [10] is a classic generic technique providing both local foci of users' attention and the overview of the global context. Tu et al. [30] proposed a multi-focus technique on Treemap nodes, which evenly enlarges selected nodes and scales down other ones with an elastic model, while constraining the relative positions of the nodes with a directed acyclic graph (DAG). The research by Liu et al. [21] takes texts of word clouds as input, providing control on item-level constraints via a force-directed model. Words granted higher importance are enlarged while preserving former relative positions.

Photo Collage. Our approach makes a collage of maps in analogy to a collage of photos. The aim of the photo collage is to construct a visually pleasing combination from a group of input images.

Rother [25] formulated the collage problem as a multi-class labeling problem and modeled it using a Markov random field and subsequently improved the work in AutoCollage [24]. Picture collage by Liu et al. [20] imitates a real-life collage style, stacking rectangle photographs onto the canvas. Han et al. [13] supported a semantic correlated layout of intact images via a property-based hierarchy of images. ImageHive [28] uses a graph-layout and a constrained centroidal Voronoi tessellation to construct the collage layout.

Yu et al. [34] built a collage layout by solving a circle packing problem by moving each Voronoi site to the center of the maximum inscribed circle of the Voronoi cell iteratively, in order to preserve maximum possible circle space for each input image.

While photos that contain circle-like salient regions benefit from the circle packing, those with more irregular shapes do not. Liu et al. [19] addressed this situation based on triangulation. Restricted by chordal axis transformation (CAT) regions, cutouts maximize their coverage rate without overlapping each other. The cells produced are not necessarily

convex and are suitable for containing cutouts with arbitrary shapes.

Existing photo collage works reflect relationship of images by adjacency, i.e, putting relevant images together. They don't need to constrain the relative position while making a compact layout.

3 Map Collage

In this section, we first define and formulate the problem. Secondly, we describe the method of high-density regions extraction. Thirdly, the procedure of constructing the map collage is introduced. **??** shows the pipeline of the map collage approach for one frame geovisualization. In section 4, we extend our work to the temporal dimension.

3.1 Problem Definition

The goal of our method is to resize a full-size geovisualization from its original display space Ω to a smaller target display space Ω'. The high-density regions of the original geovisualization is extracted and clustered to form a group of non-overlapping convex polygons, called important regions, formulated as $R = \{r_i\}_{i=1}^{n}, r_i \subseteq \Omega$.

A partition of the target space consists of a set of connected polygons called cells, formulated as $V = \{v_i\}_{i=1}^{n}, v_i \subseteq \Omega'$. Each cell is associated with specifically one important region and shows the context around that region, thus could be regarded as a viewport on the original full-size map. The viewport of a cell, indicated as $M(v)$, is a mapping from Ω' to Ω, so that moving the focusing geographical location of a cell can be considered as moving its viewport on the original map.

The final map collage on the target display space is composed of the partition and the focusing locations of cells. Overall, we identify three requirements of the map collage:

Each important region should be fully visible in its associated cell and maintain a consistent scale level. In the following paper, the intersection of an important region and its cell is defined as the *true gain*, formulated as $tg_i = A(\cap(v_i, r_i))$, where $A(r)$ denotes the size of a region.

In our work, space around important regions provides context and visual guides and shouldn't fully give way to the important regions. It's different from the works of the photo collage aiming to maximize the coverage rate of visible salient information [34], or in another word, cutouts [19]. So that the *true gain rate* is defined as $tgr_i = tg_i/A(r_i)$ and $tgr_i = 1$ given fully displayed important region. The set of true gains of all cells is indicated as $TG = \{tg_i\}_{i=1}^{n}$.

Each important region should avoid being visible display of unassociated important regions. One problem of map collage, is that when putting multiple viewports (collage cells) on a common substrate (geovisualization), a cell may show the important regions other than the associated one, causing the phenomenon illustrated in Figure 2. In another word, the viewports overlap causes the visual repeating and waste the target display space. The higher the density of the regions or the smaller the size of the target display, the more likely this problem appears.

To formulate this problem, we define the *false gain* of a cell v_i as the sum of intersected area of its viewport $M(v_i)$ and unassociated regions, indicated as $fg_i = \Sigma_{k \neq i} A(\cap(M(v_i), r_k))$. The set of false gains of all cells is indicated as $FG = \{fg_i\}_{i=1}^{n}$. Figure 1 illustrates how the true gain and the false gain are defined.

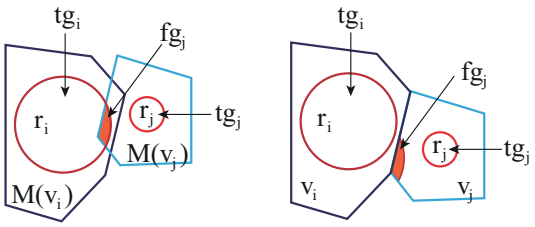

(a) Original display space (b) Target display space

Fig. 1 Illustration of the true gain and the false gain. The cells and their viewports are in blue and the important region are in red. v_i and v_j are associated respectively to r_i and r_j. The area of false gain is marked in orange, which is a segment of r_i. v_i and v_j both have 100% true gain rate for r_i and r_j, the two red circles, are fully contained in their cells. v_i has zero false gain, while v_j intersects with r_i and has false gain.

The layout should preserve relative position of neighboring important regions, which could help users to realize possible connections among geospatial data. At least, the worst situation where relative positions of two close regions are reversed is not allowed. In this paper, the relative position is that, intuitively, if in Ω, an important region r_a has a neighbor region r_b to its bottom right, then in Ω', the canvas position of r_b is assumed to also be to the approximate bottom right of r_a.

3.2 High-Density Regions Extraction

In this paper, the important regions mainly are the regions with high-density values on the density maps. It's also possible that locations interesting to a user has few geospatial data and low density. The users are allowed to manually mark locations, which can be easily supported in the pipeline.

We extract high-density regions from the density map by binary thresholding, the threshold for which is application-related and indicated as $thresh_{density}$. Its effect on the final result is displayed in Figure 10. The manually marked regions are included into the binary map at this point. Then the polygons are extracted from the binary map and clustered by density (of polygon centroids). For simplification,

we group all regions of the same cluster into one convex polygon. Allocating multiple cells to each one of a group of dense important regions causes visual repeating, which appears as a broken mirror reflecting similar views in each shard, as illustrated in Figure 2, where space is wasted showing the same geographical context repeatedly.

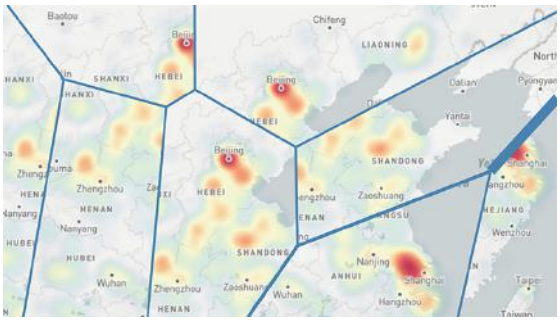

Fig. 2 Example map collage with no clustering performed when extracting density regions. Heavy visual repeating could be observed. Beijing appears in 3 cells.

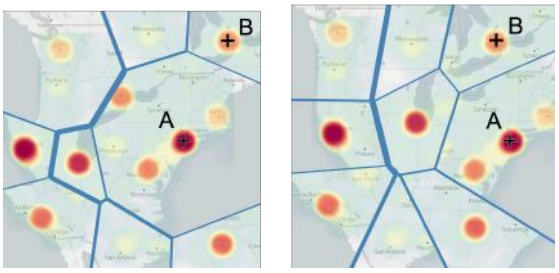

(a) Power weighted CVT (b) Our method

Fig. 3 Comparison between the collage results using the power weighted CVT (a) and using our method (b). Originally, location B is northwest of A. In (a), B is shifted to the northeast of A. In (b), the position relation is more constrained and less shifted.

Our implementation uses a contour detection algorithm [27] to extract polygons out of thresholded density maps. Polygons are clustered by DBSCAN [8] on their centroids. The *MinPts* of DBSCAN is set to 1 to allow single isolated regions to be distinguished. After clustering, a convex-hull-finding algorithm [12] is applied to each cluster of polygons, forming a new convex polygon enveloping all members of the cluster.

3.3 Layout Construction

Given the centroids of the important regions as Voronoi sites, the bounded rectangular display space could be partitioned by Voronoi diagram. The partition should be aware of the

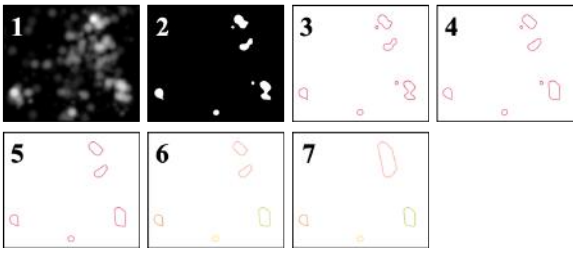

Fig. 4 The pipeline of extracting the high-density regions. (1) The density map. (2) Thresholded binary map. (3) Contour-finding. (4) Computing convex hull. (5) Size filtering (optional). (6) Density clustering. (7) Computing convex hull again.

region sizes. The weighted centroidal Voronoi tessellation (the weighted CVT) of Voronoi Treemap [4] could be used to generate a partition where the cell sizes proportional to the size of the associated important regions and the regions are evenly distributed. However, the weight CVT does not consider relative positions of the Voronoi sites, as showed in Figure 3a. The result in Figure 3b is more reasonable.

The packing algorithm, such as the circle packing algorithm is a feasible solution for the photo collage [34] but it ignores relative position of items and goes only for maximum space usage, which do not well match our requirements for the map collage. The Voronoi sites could be moved to adjust the cell positions. The algorithm is fast enough to support real-time user interaction to revise the collage layout, such as dragging to move the sub-maps closer for easier comparison.

We separate the problem into two parts, construct the collage layout in two steps:

1. Applying a force-directed relaxation on a connected graph of centroids of the important regions to adjust their positions properly for the next step. The relative positions (requirement 3) are preserved in this step.
2. Partitioning the target display space using adaptive power weighted Voronoi diagram given the centroids as Voronoi sites while taking the requirement 1 and 2 into consideration.

Before going further, the power diagram, the centroidal Voronoi diagram (CVT) and the weighted CVT are reviewed below. Only 2-D situation is mentioned here.

The power diagram [2] is a weighted Voronoi diagram using the power distance as distance measure. Given a set of points (called Voronoi sites or Voronoi generators) $P = \{p_i\}_{i=1}^{n}$ in $\mathbb{R}^2$ and their weights $W = \{w_i\}_{i=1}^{n} (w_i \leq 0)$ and the power distance measure formulated as

$$d_{pw}(q, p_i) = \|p_i - q\|^2 - w_i, \tag{1}$$

the generated power diagram is a partition of $\mathbb{R}^2$, with each cell v_i defined as

$$v_i = \{q \in \mathbb{R}^2 \mid d_{pw}(q, p_i) < d_{pw}(q, p_j), \forall p_{j \neq i} \in P\}. \tag{2}$$

The centroidal Voronoi tessellation [7] (CVT) is a kind of Voronoi diagram with evenly distributed cells with aspect ratio close to one. Lloyd's method [22] iteratively moves each site to the centroid of its cell and then recomputes the Voronoi diagram until the distance error between sites and cell centroids reaches a threshold.

The weighted version of CVT was first presented by Balzer et al. for computing Voronoi Treemaps [4], designed in analogy to Lloyd's method. Other than centering sites, the algorithm adaptively alters site weights so that the principle structure of Treemaps [14], the size of each cell being proportional to the value of the corresponding node, is satisfied.

3.3.1 Centroids Scaling

Centroids of the important regions are used as Voronoi sites to partition Ω' after that they are mapped from Ω to Ω'. There could be paddings between the bounding box containing all important regions and the boundary of Ω, So that the uniform scaling down keeps the paddings which we would like to eliminate for utilizing the space of Ω'.

Let $B(R)$ denote the bounding box of R, $C = \{c_i\}_{i=1}^{n} \subset \Omega$ the centroids of R, $P = \{p_i\}_{i=1}^{n}$ the resulting Voronoi sites in Ω'. We eliminate the paddings by scaling the centroids from $B(R)$ to Ω', formulated as

$$x(p_i) = (x(c_i) - x(B(R)_{tl}))\frac{W(B(R))}{W(\Omega)}, \forall i \in [1,n] \tag{3}$$

where $B(R)_{tl}$ is the top left point of $B(R)$, $W(B(R))$ is the width of $B(R)$, $W(\Omega)$ is the width of Ω and $x(p_i)$ is the x-coordinate of p_i. The formulation computing the y-coordinates is similar. Intuitively, the scale first aligns $B(R)$ with Ω' on the top left corner and then scales down $B(R)$ to its size.

3.3.2 Force-directed Position Adjustment

Performing size adaption with fixed-position sites could probably generate poor results depending on the distribution and weights. As illustrated in Figure 5a, sparse low-weighted sites are assigned more space than needed and cell size of the highest-weighted site is limited. We adjusts the site positions to a properer state while preserving the position relationship, achieving the result in Figure 5b.

A set of properly positioned sites should (1) keep all important regions within Ω', (2) have large interval around high-weighted sites and small interval around low-weighted ones, and (3) constrain relative positions. Three forces are designed for the three requirements: (1) the boundary force, (2) the collision force and (3) the link-direction force.

The collision force pushes sites away from each other, leaving sufficient space for cell size adaption. The shapes of important regions are taken into consideration by performing polygon collision. The polygons for collision is generated by outwardly expanding edges of the important regions until the sizes increase to $x_i, \forall i \in [1,n]$.

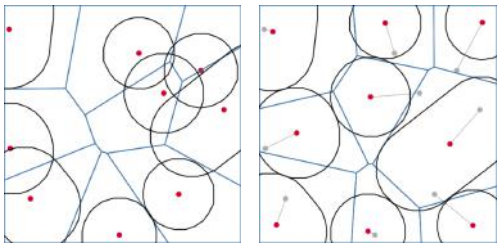

(a) (b)

Fig. 5 Results of size adaption with different site positions (in red). The black polygons represent the desired display spaces of the cell. (a) With no position adjustment, the cell on the right with the largest desired size is limited by its neighbors, while others take more space than need. (b) After position adjustment, the cell sizes are properer.

The boundary force is used to keep the important regions inside the boundary of Ω'. For any p_i, the specific boundary is the boundary of Ω' shrunk by half the width and height of the bounding boxes of r_i. Let Γ_i denote the boundary for p_i and $\Gamma_i(p_i)$ the projection of p_i onto Γ_i. If p_i is outside of Γ_i, $\Gamma_i(p_i)$ is the closest position on Γ_i from p_i. Otherwise, $\Gamma_i(p_i) = p_i$. The boundary force is formulated as

$$F_b(i) = \begin{cases} k_b \left\| \Gamma_i(p_i) - p_i \right\| & \text{, if } p_i \text{ is outside of } \Gamma_i \\ 0 & \text{, else} \end{cases} \tag{4}$$

where k_b is the weight of the boundary force.

The link-direction force is used to constrain the relative positions of the sites by keeping the direction of links among the sites from changing too much. The links are established by performing Delaunay triangulation to the sites at the beginning after they are scaled down, so that only links of neighbor sites are considered. Liu et al. [21] kept the orthogonal order of site positions by verifying their horizontal and vertical order independently. We instead apply the constraint allowing the links to shift near vertical and horizontal axes. As illustrated in Figure 6, forces are applied to both endpoints of a link to restore the original direction of it. The link-direction force is formulated as

$$\begin{aligned} F_s(i) &= \sum^{(i,j)\in E} \left\| p_i' - p_i \right\| \\ p_i' &= p_j + \mathbf{e_{ji}} \left\| p_i - p_j \right\| \end{aligned} \tag{5}$$

where E is the set of links established by Delaunay triangulation, $\mathbf{e_{ji}}$ is a unit vector denotes the original direction from j to i, and p_i' is the desired position of p_i.

3.3.3 Size Adaption

After the site positions being adjusted by the force model, the partition is generated based on the power weighted CVT.

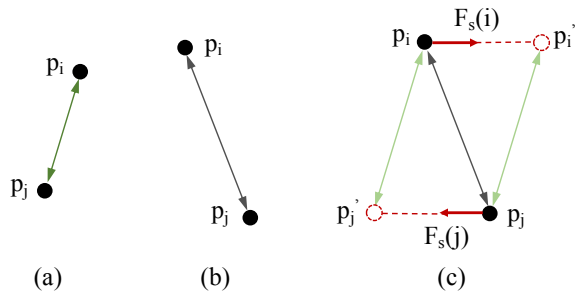

Fig. 6 Illustration of the link-direction force: (a) Original positions of sites (p_i, p_j) with link in green. (b) Positions change caused by other forces. (c) Desired positions (p_i', p_j') are computed from the original link-direction. The forces ($F_s(i)$, $F_s(j)$) pull p_i and p_j, respectively, to their desired positions.

To satisfy the desired sizes of cells, the site weights are adaptively altered in each step of the iteration. A power diagram is generated at the beginning of each step, and then the actual size of each cell is compared with its desired size. If the actual size is smaller than the desired size, the corresponding site weight is increased. If the cell is larger than desired, the weight is reduced. At the end of the step, weights are limited from being too large, otherwise nearby cells could be overwhelmed and vanish. To increase the true gain and to reduce the false gain of every cell, the site weights are multiplied by two additional scale factors, other than the desired size. Our algorithm of size adaption is outlined as subsubsection 3.3.3.

3.3.4 Map assembly and optimization

The size adaption yields the partition scheme V. Another component of the layout is the focus regions M, defined in the last of subsection 3.1. For now, the focus region of each cell locates at the centroid of it.

Due to the uncertainty of cell shapes from Voronoi diagram, an important region may not be fully contained by its cell. To maximize true gains and minimize false gains, we first optimize the layout by altering M, intuitively speaking, by panning the important region along with the map (but not rotating) inside each cell. We implement a heuristic optimization in analogy to that of the work of photo collage [34], which computes saliency losses in four quadrants to obtain a moving direction for the important region of the cell. Then, a new position of the important region is searched inside a circle in the direction.

The false gain of a cell is reduced by moving each focus region towards the false important region from which the false gain is obtained so that the false gain is moved out of the cell. A new set of focus regions M is computed. For an optimized cell, the centroids of r_i and v_i are no longer necessarily aligned. At the end of this procedure, a collage result is constructed.

Input: target display plane $\Omega' \subset \mathbb{R}^2$; important regions R; Voronoi sites P; desired sizes $X = \{x_i\}_{i=1}^n$ with $\Sigma_{i=1}^n x_i = A(\Omega')$; maximum cell size error threshold ε.
Output: partition $V(P)$ of Ω' with n cells.

initialize weights W with $w_i = 1$
repeat
  $V(P) = PowerVoronoiDiagram(\Omega', P, W)$
  Move each important region to its assigned cell
  Compute true gains TG and false gains FG
  stable=true
  for all $p_i \in P$ **do**
    $A_{current} = A(v_i)$
    $f_{desiredSize} = (x_i / A_{current})^{k_{desired}}$
    $f_{trueGain} = (1/tg_i)^{k_{tg}}$
    $f_{falseGain} = (exp(-fg_i) + k_{fg})/(k_{fg} + 1)$
    $w_i = w_i * f_{desiredSize} * f_{trueGain} * f_{falseGain}$
    $w_i = max(w_i, 1)$
    if $|A(v_i) - x_i| > \varepsilon$ **then**
      stable=false
    end if
  end for
  $f_{constrain} = \infty$
  for all $\{p_i, p_j\} \subset P$ with $i \neq j$ **do**
    $f = (\|p_i - p_j\|)^2/(w_i + w_j)$
    if $0 < f < f_{constrain}$ **then**
      $f_{constrain} = f$
    end if
  end for
  if $f_{constrain} < 1$ **then**
    for all $p_i \in P$ **do**
      $w_i = w_i * f_{constrain}$
    end for
  end if
until stable == true
return $V(P)$

3.3.5 Visual Encoding for Edges

Drawing edges between cells is essential, otherwise two adjacent cells are hard to be visually separated. A weakness of our approach is that when the cropped context brings originally distant regions much closer making it easier for users to compare, it also inevitably brings bias to the relative positions which we already tried to constrain. We try to compensate for the loss of context by indicating how much context is cropped by encoding the distance between two regions of two cells to the width of their common edge as shown in Figure 7(a).

4 Temporal Map Collage

Resizing becomes challenging when the content dynamically changes in time. Temporal-spatial density data could be regarded as a video on which the video resizing approaches can be applied. However, when a user switches from frame to frame, continual shifting of distortion also distorts users' mental map, more importantly, the inconsistent distortion on the same region is quite confusing.

If the temporal dimension is sampled at a large interval, the generated frames tend to preserve weak temporal

coherence. If the important regions vary substantially in their number, position, and size, so do the resulting collage layouts. Our strategy starts by computing a global set of important regions, from which a global map collage is constructed. Specific adjustments are made to the global collage layout for each frame generating a layout for each frame. All the layouts have a same number of cells and similar cell positions, contributing to keeping users' mental map.

4.1 Global Important regions

If a geographic region presents high density in all frames, it's naturally a hotspot. A region presenting high density in only a few frames, or even one single frame, could mean outliers deserving attention. So that we take all high-density regions of all frames into consideration. We perform an OR operation on the thresholded density maps of all frames, resulting in a global density map, instead of using average operations to generate the global density map, which would dilute density that appears in a few frames.

Extended to the temporal dimension, the set of density maps of all frames is a 3-D matrix $D = \{1,\dots,T\} \times \{1,\dots,W\} \times \{1,\dots,H\}$, where T is the temporal length of the dataset. Each 2-D slice d_t for all $t \in [1,T]$ is a frame of density map, and each element $D(t,i,j)$ is a pixel value in the range of $[0,255]$. Let the global density map be indicated as d_{global}; then, its pixel value is formulated as

$$d_{global}(i,j) = \bigcup_{t=1}^{T} \{D(t,i,j) > thresh_{density}\}. \quad (6)$$

4.2 Temporal Optimization

A global collage layout is constructed from the global density map computed by Equation 6. Applying the global collage layout may cause unwanted effects in some cases. An important region could be close to the edge of the cell and stray far from the cell center. In a rare case, an important region could show itself in more than one cells.

Our approach adapts the global collage on only the frames where the collage performs poorly, which is identified if any of the three metrics, namely, minimum true gain rate, maximum false gain rate, or maximum centroid offset exceeds its threshold. Experimentally, the three thresholds are set as 100%, 5% and 45%. The true gain rate and the false gain rate are defined in subsection 3.1. The centroid offset is the distance between the cell center and its focus region.

When the global collage layout is applied to a frame with important regions different in number, position, and size, the correspondence between important regions and cells must be re-established. Each important region is assigned to the cell that displays most of it. So that a cell could be responsible for displaying multiple regions or no region at all, while a region should appear in at most one cell.

If the maximum centroid offset of a cell exceeds the threshold, its site is moved towards the average centroid of all its responsible regions. Visually, the cell moves towards the regions, taking them into containment while pushing other cells away. The desired size of each cell is recomputed using the sum of size of its responsible regions. At a frame, to keep the size of a cell that is responsible for no region from shrinking too much, the cell holds its corresponding global region as a placeholder. Additionally, a transition animation of the layout is played when viewers switch among frames transforming the partition and panning the maps. We show the experimental results of temporal map collage in section 5.

5 Experiments

All experiments are performed on a MacBook Pro 2015 with an Intel Core i7 CPU running at 2.2 GHz and 16 GB RAM. We implemented the method in the form of a web application with JavaScript and Python. OpenCV functions are called from Python interfaces to extract polygon contours and to calculate convex hulls.

5.1 Datasets

The first dataset includes the locations and dates of *Flickr user postings*. Flickr is an online social community allowing users to upload and share photos and videos. The data came from Yahoo Flickr Creative Commons 100 Million (YFCC100m) dataset [29]. We show only density maps rendered using the posts in the mainland of the United States. The temporal range is from January 2007 to February 2014. Data of each month are rendered as a density map, resulting in totally 86 frames. The resolution of each density map is 1240*620. Density values are high in major cities such as New York, Washington D.C., San Francisco, and Chicago. Among these large cities are intervals with large spreading but low-density areas, which is ideal for constructing the map collages.

The second dataset is the *air quality index (AQI)* covering Middle and East China, the Korean Peninsula, and Japan. The dataset were obtained from the World Air Quality Index project [3], a non-profit project providing unified and global air quality information. Data of each day is rendered into a density map, resulting into 32 frames from 12 April to 13 May in 2016. The resolution of each rendered density map is also 1240*620. High-density areas appear at large cities where the pollution originates. Due to the dense distribution of pollution sources, the high-density regions are much

[3] http://aqicn.org

(a) 500×500 (b) 375×667 (c) 667×375 (d) 262×467 (e) 467×262

Fig. 7 Collage results of different target display spaces. The maps of all cells keep the same zoom level so that all important regions keep the same size.

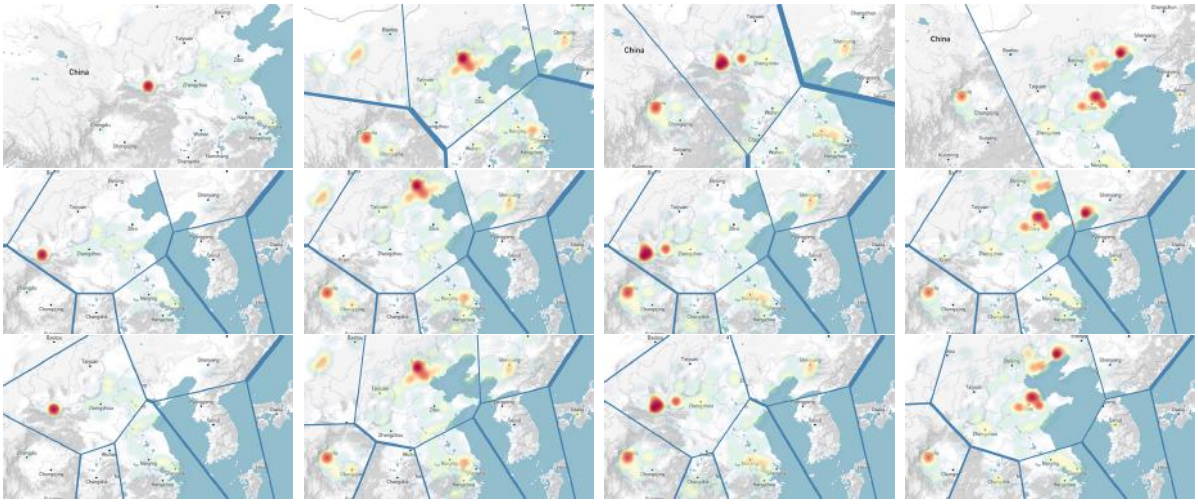

(a) (b) (c) (d)

Fig. 8 Collage results of four sequential frames, one for each column. The results of each row use (top) independent layouts, (middle) global layout, and (bottom) adapted layouts based on the global one.

closer to each other, resulting in large important regions after clustering and extraction (subsection 3.2). Because of such feature, the map collage is less suitable for working on this dataset than the former one. However, the collage result still benefits from skipping regions with low AQI, such as the Sea of Japan.

5.2 Results

The results of the map collage for one frame with different resolution and aspect ratio are displayed in Figure 7. The zoom levels of maps in cells are as same as the original geo-visualization and no additional zoom is performed. Overall, our method adapts the target space well. However, when the canvas is too small (d), the collage fails to fully contain the region at right bottom, even though there is more empty space around. The maps could be simply uniformly scaled down to solve this.

The influence of $thresh_{density}$, the threshold of binary thresholding extracting important regions (subsection 3.2), is displayed in Figure 10. Generally, the cell number decreases as $thresh_{density}$ increases as more important regions are excluded. When $thresh_{density}$ is low in Figure 10f, however, regions are dense and clustered into large regions which cannot be well contained. We found by experiment that $thresh_{density} = 150$ is appropriate for the AQI dataset and 170 for the Flickr dataset.

Figure 9 shows the comparisons among four approaches: the map collage, the power weighted CVT [4] (PWCVT for short), the seam carving [3] and the adaptive triangulation [18]. The seam carving and grid-based image resizing approaches keep the continuity of the geographical context at the cost of introducing nonlinear deformation. Figure 8

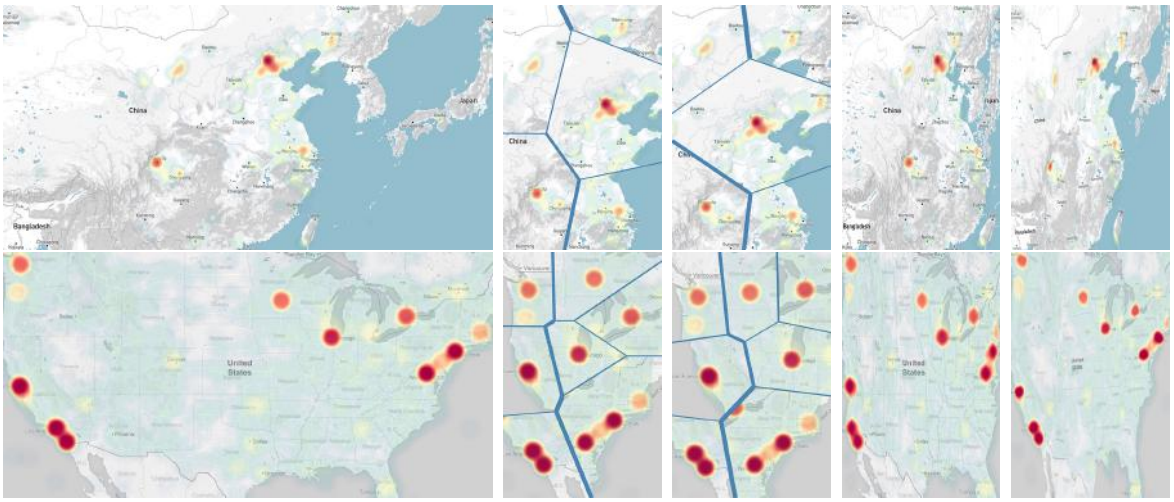

(a) Original visualization (b) Ours (c) PWCVT (d) Seam carving (e) Adaptive triangulation

Fig. 9 Results of different methods with smaller width.

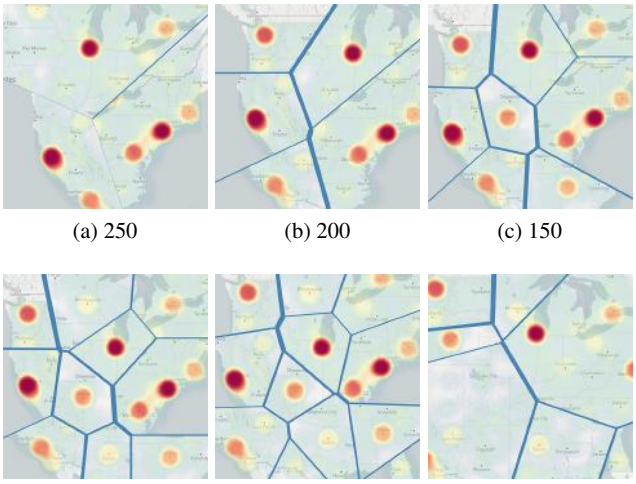

(a) 250 (b) 200 (c) 150

(d) 125 (e) 100 (f) 50

Fig. 10 Results with different density threshold $thresh_{density}$.

displays the results of temporal collage on four frames. Each column shows the same frame.

The results at the top row are generated independently and each one differs from each other too much, so that users would expend substantial effort to keep track of each region. The four at the middle row share the same global layout, with some issues described in subsection 4.2. The four at the bottom row are optimized. In each layout of the first three frames of the middle row using the global layout (Figure 8 (a, b, c)), an important region is close to the cell border and leaves a large empty space in the middle. In the right most frame (Figure 8d), an important region is split into two cells. The bottom row shows optimized layouts. In Figure 8d, the important region is contained within one cell.

6 Evaluation

We evaluated the relative-position-preserving feature by comparing angle changes of the links between our method and the power weighted CVT (PWCVT). Besides, we also evaluated the PWCVT added our size adaption (subsubsection 3.3.3) and the optimization (subsubsection 3.3.4), called the PWCVT optimized. Figure 11 shows the effectiveness of link direction preservation of our force model. On the Flickr dataset, bad situations occurred in both the PWCVT and the PWCVT optimized (opt), where the direction of link is severely disturbed (larger than 90 degrees). The relative positions on the AQI dataset generally are less disturbed than those on the Flickr dataset because the frames of the AQI dataset contain much fewer important regions than those of the Flickr dataset.

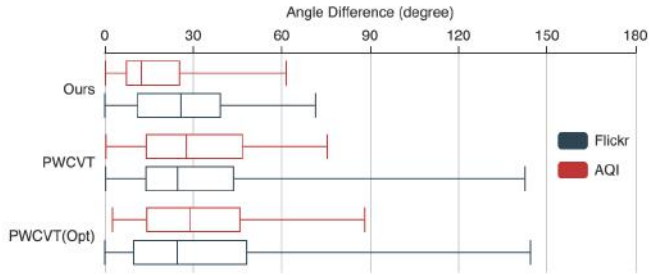

Fig. 11 Boxplots comparing the link-direction-preservation of the three methods on the two datasets, Flickr (blue) and AQI (red).

7 User Study

We conducted a user study to evaluate the ability of the map collage in enhancing the user experience of viewing geospatial data in the form of density maps. There were 20 participants with 16 of them familiar with the field of visualization. The results of the adaptive triangulation [18] shown in subsection 5.2 were not included in the study because of its inadequacy. When the visualization is resized to a similar aspect ratio, the morphing is too slight to notice, and in other conditions, the results are not as good as those of the seam carving, which can be observed in Figure 9(d,e).

We generated results on 5 frames using 3 methods in the order of the seam carving [3], the map collage and the uniform scaling, producing 15 mobile-size visualizations. The results were grouped and displayed by methods, that is saying, the participants are allowed to freely browse and revise their answers in group but not among groups.

The questionnaire was carried out on participants' private mobile phones. The results are displayed as static images, which means all regions in the results are high-density ones. The participants were asked to perform no interaction (zooming and panning) to the images and keep a natural distance from the screen. Besides, a brief introduction of the density map and the definition of the *high-density region* were given at the beginning.

The participants were asked to finish 2 tasks: (**T1**) *compare two high-density regions and determine which of them is actually larger despite the visual deformation;* (**T2**) *identify the number of high-density regions.* Our assumption is that the nonlinear deformation of the seam carving would bring misinterpretation in both tasks, especially **T1**. Using the uniform scaling, users are expected to perform similar as using the map collage but taking more efforts. In the end, the participants were asked to give their preference of the three methods. We assume that the map collage is more preferred than the uniform scaling for the saved efforts.

The results are summarized in Figure 12. The average spent time on the questionnaire is 6 minutes. The results of **T1** show that the participants made more mistakes using the seam carving (Figure 12a) and were more certain of their wrong decisions than the right ones (Figure 12c), although the participants felt approximately equally certain of the three methods (Figure 12b). The results of the uniform scaling, on the other hand, varies not much from ours. For **T2**, the absolute errors between the real counts of high-density regions and users' answers show that the users are closer to the accurate value using our map collage than the other two, suggesting less misleading on this task. Given the 2 tasks, most participants preferred using the map collage. Overall, the results confirm our beforehand assumption.

Most participants appreciated that the collage layout saves their efforts to observe and compare the high-density regions, while some were concerned that its non-continuity prevents users from obtaining a global understanding and would bring misinterpretation on holistic tasks.

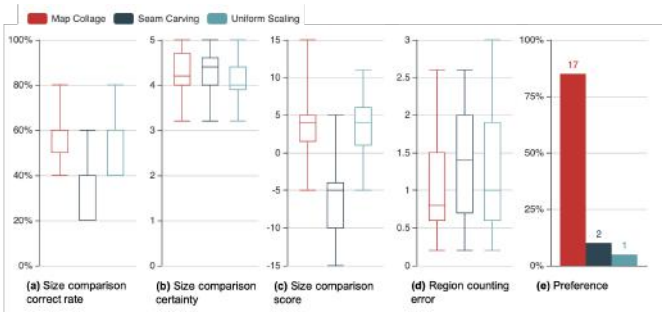

Fig. 12 Results of the user study. (a) T1 correct rate. (b) T1 certainty level. (c) T1 score: correctness (1 for correctness / -1 for incorrectness) $*$ certainty level. (d) T2 absolute error. (e) Votes for the preference.

8 Limitations and Discussions

The non-continuity of the map is an inevitable shortcoming of our approach. The loss of continuous information among sub-maps would impair users' performance on holistic tasks such as (1) understanding of the global data distribution, (2) navigating among geographical locations. So it's better if the map collage and the original geovisualization coexists in application scenarios. In a mobile application, a map of overview could appear as a mini-map at the corner or a called-by-interaction layer of the application. Or the map collage could appear as an auxiliary view for the full-size geovisualization.

Another resizing approach could be a multi-focus deformation which enlarges the important regions with a consistent scale and introduces no deformation to them, which is the point of our work. Meanwhile the other non-important regions are deformed to give space and preserve continuous information. The approach has some weaknesses. First, it is hard to cope with vector graphics while our pipeline considers them as same as raster images. Second, it is not easy to be extended to the temporal dimension while handling the deformation smoothly. Our method only applies to sparsely distributed density map. Third, user may miss some unimportant regions if our approach is applied. Fourth, map-interaction is not abundant.

9 Conclusion

The proposed map collage crops and stitches maps to resize the geovisualizations to smaller displays, while pulling the important regions closer for easier comparing and preserving

their sizes and relative positions. The map collage presents a deformation-free way of resizing the geovisualizations, compared with other resizing techniques that introduce morphing to the image-based underlying map. A user study was conducted showing that the map collage performs better than the seam-carving and the uniform scaling for the tasks of comparing high-density region sizes and counting the number of them. A simple strategy shows that the collage layout could be extended to the temporal dimension allowing for browsing geotemporal data.

Future works include trying other 2-D plane partition techniques and conducting more evaluations seeking better capacity and effectiveness of the collage layout. We would explore more application scenarios or visualization forms, such as scatterplots, with which our proposed method could cope. In addition, collaging map for the streaming data is another potential work. Without knowing the knowledge of yet coming next frame of streaming data, the layout might be required to change drastically in the new approach.

Acknowledgements This work was supported by the National Natural Science Foundation of China under Grants (No. 61672237, 61532002, 61802128) and the Fundamental Research Funds for the Central Universities.

References

1. Aitchison, A.: The google maps/bing maps spherical mercator projection. Available onine: http://alastairawordpresscom/2011/01/23/the-google-maps-bing-maps-spherical-mercator-projection/(accessed on 14 April 2014) (2011)
2. Aurenhammer, F.: Power diagrams: properties, algorithms and applications. SIAM Journal on Computing **16**(1), 78–96 (1987)
3. Avidan, S., Shamir, A.: Seam carving for content-aware image resizing. ACM Transactions on Graphics (TOG) **26**(3), 10 (2007)
4. Balzer, M., Deussen, O.: Voronoi treemaps. In: IEEE Symposium on Information Visualization, 2005. INFOVIS 2005., pp. 49–56 (2005)
5. Buchin, K., Speckmann, B., Verdonschot, S.: Evolution strategies for optimizing rectangular cartograms. In: International Conference on Geographic Information Science, pp. 29–42. Springer (2012)
6. Dorling, D.: Area cartograms: Their use and creation, concepts and techniques in modern geography (1996)
7. Du, Q., Faber, V., Gunzburger, M.: Centroidal voronoi tessellations: Applications and algorithms. SIAM review **41**(4), 637–676 (1999)
8. Ester, M., Kriegel, H.P., Sander, J., Xu, X., et al.: A density-based algorithm for discovering clusters in large spatial databases with noise. In: KDD 1996, vol. 96, pp. 226–231 (1996)
9. Evans, W., Felsner, S., Kaufmann, M., Kobourov, S.G., Mondal, D., Nishat, R.I., Verbeek, K.: Table cartograms. In: European Symposium on Algorithms, pp. 421–432. Springer (2013)
10. Furnas, G.W.: Generalized fisheye views. SIGCHI Bull. **17**(4), 16–23 (1986)
11. Gastner, M.T., Newman, M.: From the cover: Diffusion-based method for producing density-equalizing maps. Proceedings of the National Academy of Sciences of the United States of America **101 20**, 7499–504 (2004)
12. Graham, R.L., Yao, F.F.: Finding the convex hull of a simple polygon. Journal of Algorithms **4**(4), 324–331 (1983)
13. Han, X., Zhang, C., Lin, W., Xu, M., Sheng, B., Mei, T.: Tree-based visualization and optimization for image collection. IEEE Transactions on Cybernetics **46**(6), 1286–1300 (2016)
14. Johnson, B., Shneiderman, B.: Tree-maps: a space-filling approach to the visualization of hierarchical information structures. In: Proceeding Visualization '91, pp. 284–291 (1991)
15. Keim, D.A., North, S.C., Panse, C.: Cartodraw: a fast algorithm for generating contiguous cartograms. IEEE Transactions on Visualization and Computer Graphics **10**(1), 95–110 (2004)
16. Keim, D.A., Panse, C., Sips, M., SC, N.: Pixelmaps: a new visual data mining approach for analyzing large spatial data sets. In: Third IEEE International Conference on Data Mining, pp. 565–568 (2003)
17. Lampe, O.D., Hauser, H.: Interactive visualization of streaming data with kernel density estimation. In: 2011 IEEE Pacific Visualization Symposium, pp. 171–178 (2011)
18. Li, C., Baciu, G., Wang, Y., Zhang, X.: Fast content-aware resizing of multi-layer information visualization via adaptive triangulation. Journal of Visual Languages & Computing **45**, 61–73 (2018)
19. Liu, L., Zhang, H., Jing, G., Guo, Y., Chen, Z., Wang, W.: Correlation-preserving photo collage. IEEE Transactions on Visualization and Computer Graphics **24**(6), 1956–1968 (2018)
20. Liu, T., Wang, J., Sun, J., Zheng, N., Tang, X., Shum, H.Y.: Picture collage. IEEE Transactions on Multimedia **11**(7), 1225–1239 (2009)
21. Liu, X., Shen, H.W., Hu, Y.: Supporting multifaceted viewing of word clouds with focus+ context display. Information Visualization **14**(2), 168–180 (2015)
22. Lloyd, S.: Least squares quantization in pcm. IEEE Transactions on Information Theory **28**(2), 129–137 (1982)
23. Nusrat, S., Kobourov, S.: The state of the art in cartograms. In: Computer Graphics Forum, vol. 35, pp. 619–642. Wiley Online Library (2016)
24. Rother, C., Bordeaux, L., Hamadi, Y., Blake, A.: Autocollage. ACM Transactions on Graphics (TOG) **25**(3), 847–852 (2006)
25. Rother, C., Kumar, S., Kolmogorov, V., Blake, A.: Digital tapestry [automatic image synthesis]. In: 2005 IEEE Computer Society Conference on Computer Vision and Pattern Recognition (CVPR'05), vol. 1, pp. 589–596 (2005)
26. Rubinstein, M., Shamir, A., Avidan, S.: Improved seam carving for video retargeting. ACM Transactions on Graphics (TOG) **27**(3), 16:1–16:9 (2008)
27. Suzuki, S., et al.: Topological structural analysis of digitized binary images by border following. Computer vision, graphics, and image processing **30**(1), 32–46 (1985)
28. Tan, L., Song, Y., Liu, S., Xie, L.: Imagehive: Interactive content-aware image summarization. IEEE Computer Graphics and Applications **32**(1), 46–55 (2011)
29. Thomee, B., Shamma, D.A., Friedland, G., Elizalde, B., Ni, K., Poland, D., Borth, D., Li, L.J.: Yfcc100m: The new data in multimedia research. Commun. ACM **59**(2), 64–73 (2016)
30. Tu, Y., Shen, H.W.: Balloon focus: a seamless multi-focus+context method for treemaps. IEEE Transactions on Visualization and Computer Graphics **14**(6), 1157–1164 (2008)
31. Wang, Y.S., Tai, C.L., Sorkine, O., Lee, T.Y.: Optimized scale-and-stretch for image resizing. ACM Transactions on Graphics (TOG) **27**(5), 118:1–118:8 (2008)
32. Wolf, L., Guttmann, M., Cohen-Or, D.: Non-homogeneous content-driven video-retargeting. In: 2007 IEEE 11th International Conference on Computer Vision, pp. 1–6 (2007)
33. Wu, Y., Liu, X., Liu, S., Ma, K.L.: Visizer: A visualization resizing framework. IEEE Transactions on Visualization and Computer Graphics **19**(2), 278–290 (2013)
34. Yu, Z., Lu, L., Guo, Y., Fan, R., Liu, M., Wang, W.: Content-aware photo collage using circle packing. IEEE Transactions on Visualization and Computer Graphics **20**(2), 182–195 (2014)